NASA / TM—1998-206974 AIAA–95–0032

Flowfield Measurements in a Slot-Bled Oblique Shock-Wave and Turbulent Boundary-Layer Interaction

D.O. Davis, B.P. Willis, and W.R. Hingst
Lewis Research Center, Cleveland, Ohio

April 1998

The NASA STI Program Office . . . in Profile

Since its founding, NASA has been dedicated to the advancement of aeronautics and space science. The NASA Scientific and Technical Information (STI) Program Office plays a key part in helping NASA maintain this important role.

The NASA STI Program Office is operated by Langley Research Center, the Lead Center for NASA's scientific and technical information. The NASA STI Program Office provides access to the NASA STI Database, the largest collection of aeronautical and space science STI in the world. The Program Office is also NASA's institutional mechanism for disseminating the results of its research and development activities. These results are published by NASA in the NASA STI Report Series, which includes the following report types:

- TECHNICAL PUBLICATION. Reports of completed research or a major significant phase of research that present the results of NASA programs and include extensive data or theoretical analysis. Includes compilations of significant scientific and technical data and information deemed to be of continuing reference value. NASA's counterpart of peer-reviewed formal professional papers but has less stringent limitations on manuscript length and extent of graphic presentations.

- TECHNICAL MEMORANDUM. Scientific and technical findings that are preliminary or of specialized interest, e.g., quick release reports, working papers, and bibliographies that contain minimal annotation. Does not contain extensive analysis.

- CONTRACTOR REPORT. Scientific and technical findings by NASA-sponsored contractors and grantees.

- CONFERENCE PUBLICATION. Collected papers from scientific and technical conferences, symposia, seminars, or other meetings sponsored or cosponsored by NASA.

- SPECIAL PUBLICATION. Scientific, technical, or historical information from NASA programs, projects, and missions, often concerned with subjects having substantial public interest.

- TECHNICAL TRANSLATION. English-language translations of foreign scientific and technical material pertinent to NASA's mission.

Specialized services that complement the STI Program Office's diverse offerings include creating custom thesauri, building customized data bases, organizing and publishing research results . . . even providing videos.

For more information about the NASA STI Program Office, see the following:

- Access the NASA STI Program Home Page at ***http://www.sti.nasa.gov***

- E-mail your question via the Internet to help@sti.nasa.gov

- Fax your question to the NASA Access Help Desk at (301) 621-0134

- Telephone the NASA Access Help Desk at (301) 621-0390

- Write to:
  NASA Access Help Desk
  NASA Center for AeroSpace Information
  800 Elkridge Landing Road
  Linthicum Heights, MD 21090-2934

NASA / TM—1998-206974 AIAA–95–0032

Flowfield Measurements in a Slot-Bled Oblique Shock-Wave and Turbulent Boundary-Layer Interaction

D.O. Davis, B.P. Willis, and W.R. Hingst
Lewis Research Center, Cleveland, Ohio

Prepared for the
33rd Aerospace Sciences Meeting and Exhibit
sponsored by the American Institute of Aeronautics and Astronautics
Reno, Nevada, January 9–12, 1995

National Aeronautics and
Space Administration

Lewis Research Center

April 1998

Acknowledgments

The authors would like to gratefully acknowledge Mr. T. Bencic of NASA Lewis Research Center for matters concerning the pressure-sensitive paint technique.

Available from

NASA Center for Aerospace Information
800 Elkridge Landing Road
Linthicum Heights, MD 21090-2934
Price Code: A03

National Technical Information Service
5287 Port Royal Road
Springfield, VA 22100
Price Code: A03

FLOWFIELD MEASUREMENTS IN A SLOT-BLED OBLIQUE SHOCK-WAVE AND TURBULENT BOUNDARY-LAYER INTERACTION

D. O. Davis*, B. P. Willis*, and W. R. Hingst*
NASA Lewis Research Center, Cleveland, Ohio

Abstract

An experimental investigation was conducted to determine the flowfield inside a bleed slot used to control an oblique shock-wave and turbulent boundary-layer interaction. The slot was oriented normal to the primary flow direction and had a width of 1.0 cm (primary flow direction), a length of 2.54 cm, and spanned 16.5 cm. The approach boundary layer upstream of the interaction was nominally 3.0 cm thick. Two operating conditions were studied: M=1.98 with a shock generator deflection angle of 6º and M=2.46 with a shock generator deflection angle of 8º. Measurements include surface and flowfield static pressure, Pitot pressure, and total mass-flow through the slot. The results show that despite an initially two-dimensional interaction for the zero bleed-flow case, the slot does not remove mass uniformly in the spanwise direction. Inside the slot, the flow is characterized by two separation regions which significantly reduce the effective flow area. The upper separation region acts as an aerodynamic throat resulting in supersonic flow through much of the slot.

Nomenclature

A	=	area
D	=	slot width
H_{inc}	=	incompressible shape factor
L	=	slot length
$\dot{m}$	=	mass-flow rate
$\dot{m}'_{bl}$	=	unit mass-flow rate in boundary-layer
$\overline{\dot{m}}$	=	normalized mass-flow rate
M	=	Mach number
P	=	static pressure
P_t	=	total pressure
P_{t2}	=	Pitot pressure
$\overline{P}_w$	=	normalized wall static pressure
Q	=	sonic flow coefficient
Re	=	Reynolds number
S	=	slot span
T_t	=	total temperature
x,y,z	=	cartesian coordinate system
x_{slot}	=	distance from nozzle exit to slot l.e.
α	=	shock generator deflection angle
γ	=	ratio of specific heats
δ	=	boundary-layer thickness
δ^*	=	displacement thickness
θ	=	momentum thickness
ρ	=	density

Subscripts

0	=	condition in wind-tunnel plenum
1	=	condition in Zone 1
2	=	condition in Zone 2
3	=	condition in Zone 3
cl	=	centerline condition
i	=	inviscid condition
ref	=	condition at upstream reference plane
w	=	condition at wall

Introduction

PREVENTION or control of boundary-layer separation resulting from a shock-wave and boundary-layer interaction can be achieved by removing low momentum fluid (boundary-layer mass) near the surface through a porous region.[1, 2] The porous region may be a series of discrete perforations (holes) or a single slot. Numerical analysis of the interaction region can be very costly in terms of computer time and grid generation if the flow through the individual holes or the slot is endeavored. This is especially true if the interaction is part of a full supersonic inlet calculation. To avoid this, a global bleed model is sought which eliminates the need for resolving the bleed flow passages. An effective global bleed model should do two things: predict the amount of mass removed from the boundary-layer and predict the condition of the boundary-layer downstream of the interaction. The former is important from the standpoint of bleed drag and bleed system scaling while the latter is an indication of the effectiveness of the bleed on maintaining a "healthy" boundary-layer. To achieve these goals, the local flow phenomena in the interaction region including the bleed passages and bleed plenum must be understood and accounted for in a model. Not surprisingly, previous investigations resolving the flow through bleed passages have been computational in nature. Hamed *et al.* have studied the oblique shock-wave and laminar boundary-layer interaction with bleed through normal slots,[3] and the

*Research Engineer, Inlet, Duct, and Nozzle Flow Physics Branch.

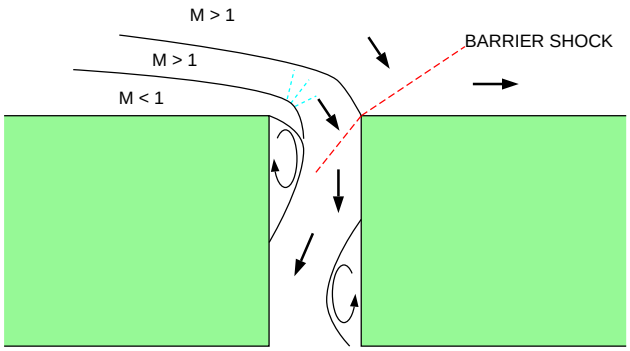

Fig. 1 Schematic of bleed interaction region (no scale).

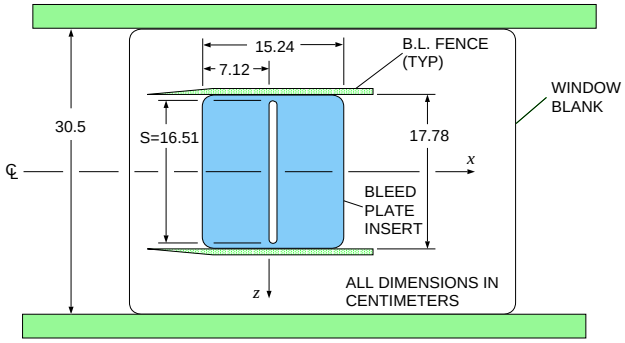

Fig. 3 Plan view of slot bleed experiment.

oblique shock-wave and turbulent boundary-layer interaction with bleed through various normal[4–6] and slanted[5, 7] slots. Because the slot configuration is two-dimensional, Hamed *et al.* were able to perform a fairly comprehensive parametric study including the effects of bleed mass-flow rates, slot location relative to shock impingement location, slot inclination angle, and slot length-to-width ratio. Hahn *et al.*[8] also numerically studied the oblique shock-wave and turbulent boundary-layer interaction with bleed through normal slots and in addition to investigating various shock impingement locations and slot length-to-width ratios included the effects of two slots with various streamwise spacing. Rimlinger, Shih and Chyu[9–12] considered the more complex (three-dimensional) case of oblique shock-wave and turbulent boundary-layer interactions with bleed through holes. These numerical studies have identified several important features of the bleed interaction. Among them are the presence of separation region(s) in the bleed passage which have a large effect on the flow coefficient of the hole or slot[13] and the presence of a two-segment barrier shock (see Fig. 1) which may or may not be attached depending on local flow conditions. Although these studies have provided a significant increase in the understanding of the shock-wave and boundary-layer interaction with bleed, unfortunately there has been no experimental flowfield data with which to compare. The present experimental investigation was undertaken in order to gain further insight into the slot-bled oblique shock-wave and turbulent boundary-layer interaction and to provide validation data for CFD methods.

Experimental Program

A schematic of the slot bleed experiment with reference coordinates is shown in Figs. 2 and 3. The bleed model is a single 90° slot, 1.00 cm wide (D) and 2.54 cm long (L) as shown in Fig. 2 and spanning 16.51 cm

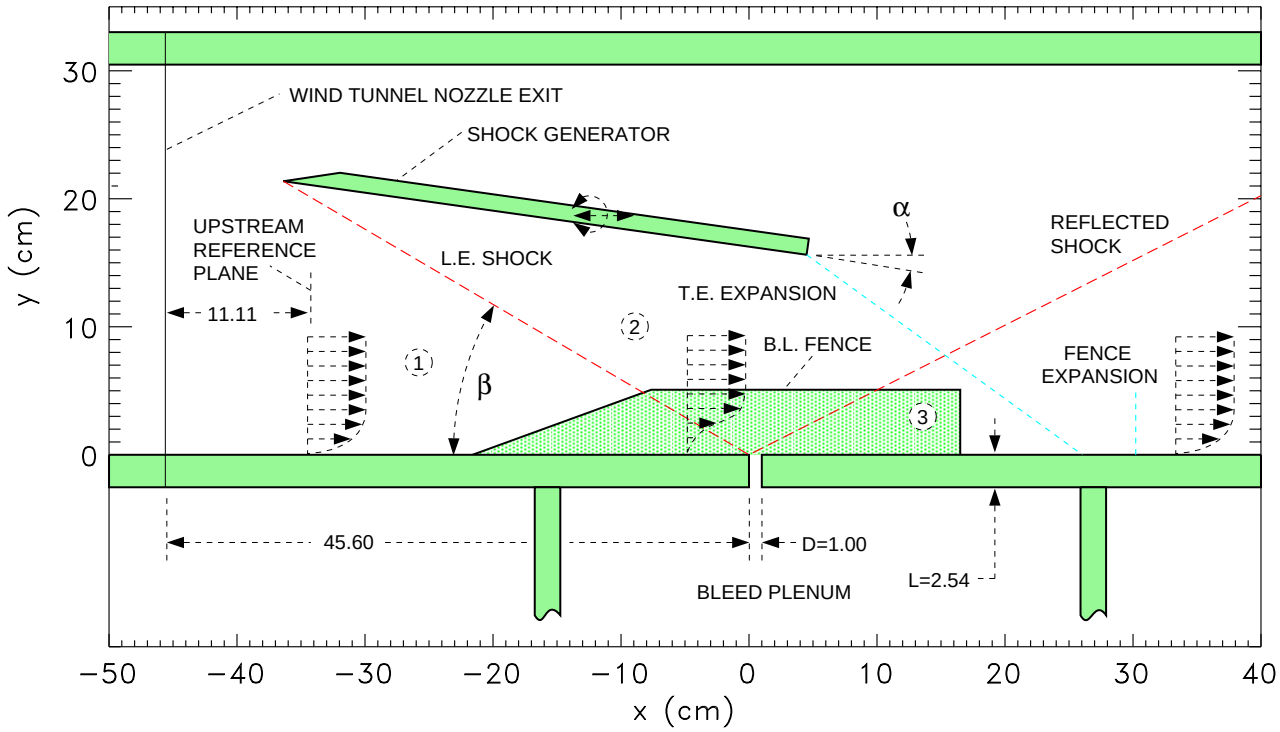

Fig. 2 Slot bleed experiment schematic.

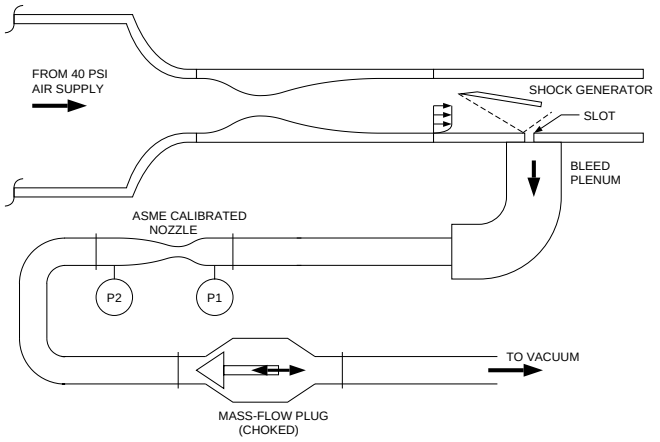

Fig. 4 Slot bleed experiment wind-tunnel schematic.

(S) as shown in Fig. 3. As indicated in Fig. 2, an oblique shock-wave is generated by a rotatable and translatable (x-direction) sharp-edged plate (shock generator). The shock generator spans the full width (30.5 cm) of the wind-tunnel. For a given deflection angle (α), the shock generator is translated until an inviscid shock-wave originating at the generator leading edge will impinge on the upstream edge of the slot. For the purpose of setting the axial position of the shock generator, the shock angle (β) is calculated based on the core Mach number measured in the upstream reference plane indicated in Fig. 2. Boundary-layer fences were used to isolate the wind tunnel test section corner flow from the interaction region.

The experiments were performed in the NASA Lewis Research Center 1X1 ft. Supersonic Wind Tunnel (SWT) which is a continuous-flow facility with Mach number variation provided by replaceable nozzle blocks. A schematic of the 1X1 SWT experiment is shown in Fig. 4. The approach boundary-layer is the naturally occurring boundary-layer on the wind tunnel wall. The oblique shock-wave interacts with the boundary-layer and a portion of the resulting distorted boundary-layer is removed through the bleed slot. The bleed flow exhausts into a large plenum where the plenum static pressure is recorded. The bleed flow rate was measured with calibrated ASME nozzles and the rate of mass-flow was controlled by a choked mass-flow plug. Bleed vacuum was supplied by lab-wide altitude exhaust and a 450 psi air ejector system.

Data were obtained for two wind-tunnel operating conditions. These conditions are referred to by the wind-tunnel core Mach number measured in the upstream reference plane (see Fig. 2). Table 1 summarizes the wind-tunnel plenum condition and the boundary-layer characteristics measured in the reference plane for each of the reference Mach numbers. The unit Reynolds number reported in this table is based on the plenum conditions and the reference plane core Mach number (M_{ref}). For the M_{ref}=1.98 condition, the shock generator deflection angle was set at α=6° and for the M_{ref}=2.46 condition, the deflection angle was set at α=8°. Previous

Table 1 Wind-tunnel operating conditions.

	M_{ref}	
	1.98	2.46
$P_{t,0}$ kPa	138.0	172.4
$T_{t,0}$ °K	293.0	293.0
$Re \times 10^{-7}$ /m	1.77	1.75
δ_{ref} cm	2.62	3.06
δ^*_{ref} cm	0.565	0.712
θ_{ref} cm	0.201	0.196
H_{inc}	1.262	1.260
$C_{f,ref} \times 10^3$	1.50	1.29
$\dot{m}'_{bl,ref}$ kg/s/cm	0.04047	0.03768

experience[14] has shown that for both of these cases the shock strength is sufficient to separate the wind-tunnel boundary-layer. Hereafter, the two cases will be referred to by the M198A6 and M246A8 designations.

Instrumentation

The experiment was instrumented to measure surface and flowfield static pressure, flowfield Pitot pressure, and the total mass-flow through the slot. All flowfield measurements were made in the z=0 plane of symmetry using conventional (intrusive) pressure probes. Because it was recognized that there would be large gradients and flow angles in the slot, efforts were made to choose instrumentation least sensitive to these conditions. However, as with all forms of intrusive type probes, inherent errors are introduced into the measurements which are very difficult to quantify. Regions of the flow that the authors believe to have a high level of uncertainty are accordingly identified.

All pressures were measured with a Pressure Systems Incorporated electronic scanned pressure system using various range transducers. All of the PSI transducers have a manufacturers quoted accuracy of ±0.07% of full-scale span.

Surface Static Pressure

Surface static pressure data were measured with pressure sensitive paint and with conventional static pressure taps. The pressure sensitive paint data were acquired using the technique described by Bencic.[15]

The tap data were measured with ±5 psi range pressure transducers which yield an absolute accuracy of δP_w=±0.048 kPa (0.007 psi).

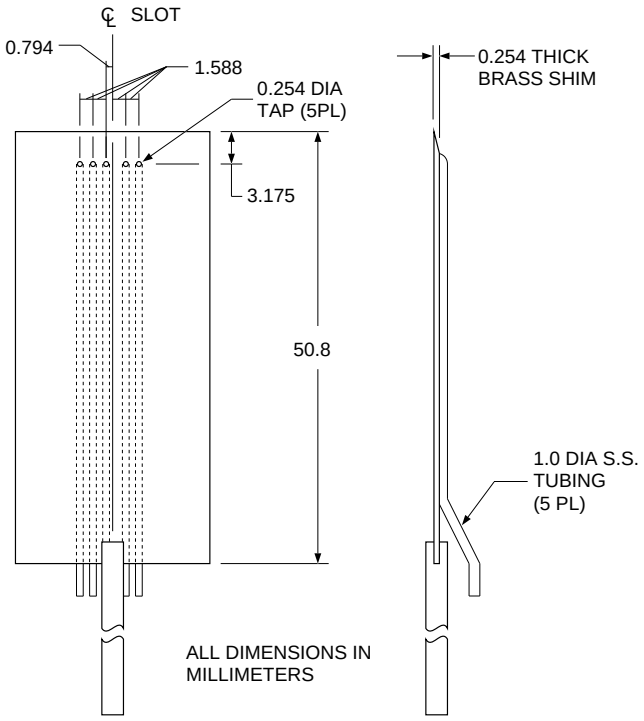

Fig. 5 Knife–edged static pressure probe detail.

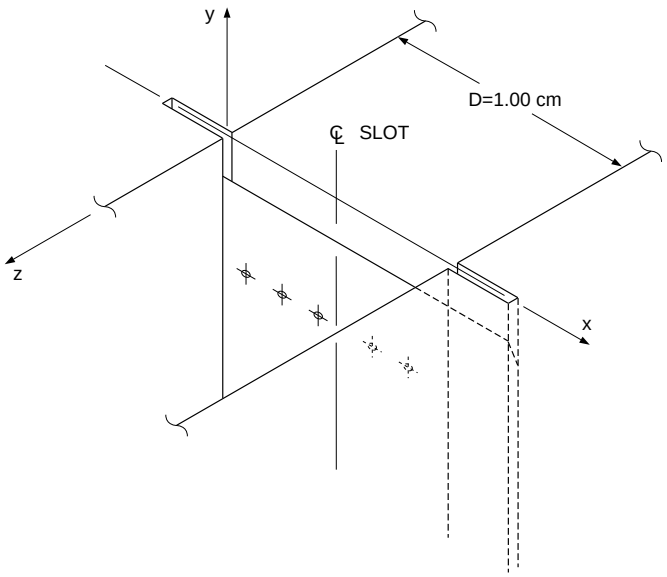

Fig. 6 Knife–edged static pressure probe installation.

Flowfield Static Pressure

Flowfield static pressure data were measured using a knife-edged probe as shown in Fig. 5 and 6. For the purpose of measuring flowfield static pressure, a special bleed plate insert was fabricated which had small grooves machined along the vertical interior surfaces of the slot on the centerline as shown in Fig. 6. These grooves serve as a guide for the knife–edged probe whose details are shown in Fig. 5. Five 0.254 mm diameter static pressure taps are located on a 0.254 mm thick sharp-edged brass shim. The taps are offset from the slot centerline such that a reversal (180° rotation about the stem) of the probe in the guides will yield data between the original tap positions for a total of ten data points in the x-direction. The probe was zeroed with the center of the taps lying in the y=0 plane (wind-tunnel surface). A remotely controlled actuator in the bleed plenum then pulled the probe through the slot. Knife-edged probes are known to be very sensitive to yaw misalignment.[16] However, since all of the data taken were confined to the plane of symmetry and the machined guides prevented aerodynamic deflection of the probe, the errors due to yaw misalignment were minimized.

Like the surface static pressure, the flowfield static pressure data were measured with ±5 psi range pressure transducers which yield an absolute accuracy of δP=±0.048 kPa (0.007 psi).

Pitot Pressure

Pitot pressure measurements were made with a 0.508 mm diameter square-edged round Pitot tube probe having an inner-to-outer diameter ratio of 0.4. Based on data presented by Bryer and Pankhurst,[16] the critical angle for this probe configuration is ±15° for incompressible flow and slightly larger for supersonic flow. Calibration of the probe in a Mach 2.0 stream showed that the probe would read within 2% of the actual Pitot pressure for pitch angles as high as ±20°. The probe was actuated from the bleed plenum in the x and y-directions.

The flowfield Pitot pressure data were measured with ±15 psi range pressure transducers which yield an absolute accuracy of δP_{t2}=±0.145 kPa (0.021 psi).

Total Mass-Flow

The total mass-flow through the slot was measured with an ASME flow nozzle. The flow rate is determined from a semi-empirical relation which gives the mass-flow as a function of nozzle geometry, temperature, upstream pressure and the pressure drop across the nozzle. A description and uncertainty analysis of this system is given by Willis *et al.*[17] For the present measurements, the uncertainty is estimated to be between ±2.20% of the calculated mass-flow.

Results and Discussion

Sonic Flow Coefficient

Numerical simulations of a bleed region utilizing a global bleed model must specify the bleed mass flow, which usually varies with local flow conditions, as a boundary condition. The mass flow may be determined from semi-empirical relations or from an experimental table look-up for a given bleed configuration. The ability of a bleed configuration to remove mass from the

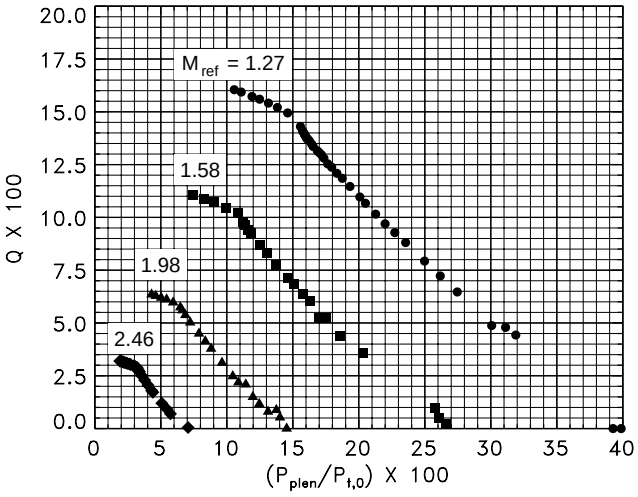

Fig. 7 Sonic flow coefficient distributions, α=0.

boundary-layer is typically quantified by the sonic flow coefficient:

$$Q = \frac{\dot{m}}{\dot{m}_{ideal,choked}} \tag{1}$$

which is usually presented as a function of the ratio of bleed plenum static pressure to freestream total pressure. Sonic flow coefficient distributions were measured for the case of an undistorted approach boundary-layer (α=0°) for four reference Mach numbers and are shown in Fig. 7. These data are presented here for reference and can be used to validate flow coefficient models for use in CFD methods. A comprehensive discussion of flow coefficient behavior for the present slot and other bleed configurations is given by *Willis et al.*[17]

When an oblique shock-wave is positioned upstream of the slot, the local Mach number in the vicinity of the slot is reduced from the upstream reference value and a shift to a different flow coefficient curve occurs. An interesting feature in Fig. 7 is the presence of a distinct kink in all of the flow coefficient distributions. This is the location where choked flow occurs in the slot. The effective throat area, however, is determined by the size of the separation region (see Fig. 1), which can vary with local flow conditions. Lowering the plenum pressure below this choke point causes an increase in effective throat area and more mass is passed through the slot.

Surface Static Pressure

Pressure sensitive paint was applied to the bleed plate insert shown in Fig. 3. Initially, it was thought that with the boundary-layer fences and the relatively large span-to-width ratio (S/D = 16.5) of the slot, that the interaction near the center of the slot would be nearly two-dimensional. For the case of no bleed flow, this was indeed the case. However, when the bleed flow was non-zero, the interaction became more three-dimensional. This behavior is illustrated by the surface static pressure obtained with the pressure sensitive paint and shown in Figs. 8 and 9 which correspond to the M198A6 case and the M246A8 case, respectively. In these figures, the lower half of the plot corresponds to the no-bleed case and the upper half corresponds to the highest bleed flow rate attainable with the bleed system. The bleed rates are given as a normalized mass-flow defined as:

$$\overline{\dot{m}} = \frac{100 \cdot \dot{m}}{(S) \cdot \left(\dot{m}'_{bl,ref}\right)} \tag{2}$$

where $\dot{m}'_{bl,ref}$ is the unit boundary-layer mass flow in the upstream reference plane (see Table 1) and S is the spanwise dimension of the slot (see Fig. 3). While the data for each flow rate are shown for only half of the bleed plate, results were obtained across the entire plate and exhibited a high degree of symmetry about the wind tunnel centerline (z=0).

For the cases with no bleed flow (the lower half of Figs. 8 and 9), the results indicate a reasonably two-dimensional flowfield except in the vicinity of the slot ends. As the bleed flow-rate is increased, the upstream influence of the shock-wave decreases, but not uniformly across the span of the slot. At the center of the slot (z=0), the upstream influence is significantly less than at the slot ends. This spanwise variation of upstream influence indicates that more mass flow is removed near the center of the slot. Although the interaction is not two-dimensional, the results were observed to be symmetric about the wind tunnel centerline (z=0 plane) and are still cogent for a three-dimensional validation case.

Conventional surface static taps were located axially on the wind-tunnel centerline through the interaction region. Normalized centerline static pressure distributions for three bleed rates are shown in Figs. 10 and 11 for the M198A6 and M246A8 cases, respectively. The normalized wall pressure is defined as:

$$\overline{P}_w = \frac{(P_w - P_{1,i})}{(P_{3,i} - P_{1,i})} \tag{3}$$

where i denotes the inviscid no-bleed condition. In these plots, the symbols represent data from the conventional surface pressure taps and the solid lines represent data deduced from the pressure sensitive paint. The theoretical inviscid distribution for the no-bleed case is also represented in these plots. The layout sketch at the top of the figures shows the inviscid no-bleed wave structure. The three bleed rates shown represent the no-bleed, maximum bleed attainable for the configuration, and an arbitrary bleed rate between the two extremes.

From Figs. 10 and 11, the following observations can be made:

1. The upstream influence of the shock-wave and boundary-layer interaction is reduced by approximately 1.5 cm for the M198A6 case and by approximately 2.5 cm for the M246A8 case when bleed is applied. This is presumably due to the removal or reduction of the separated region.

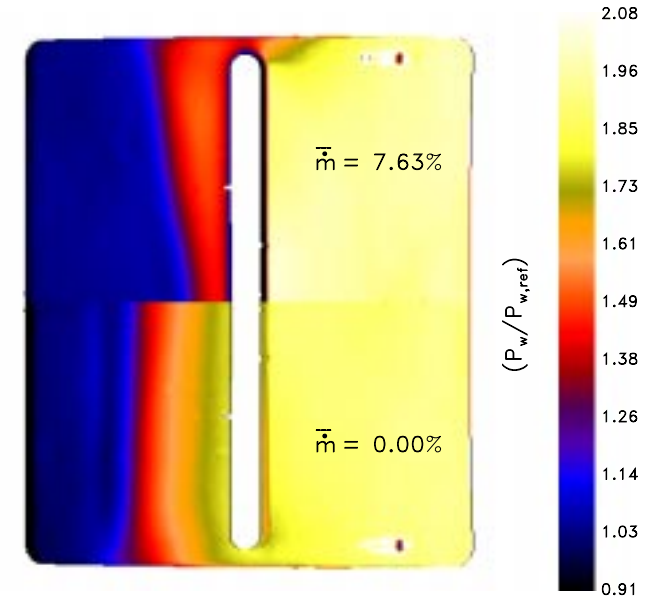

Fig. 8 Surface static pressure from pressure sensitive paint, case M198A6.

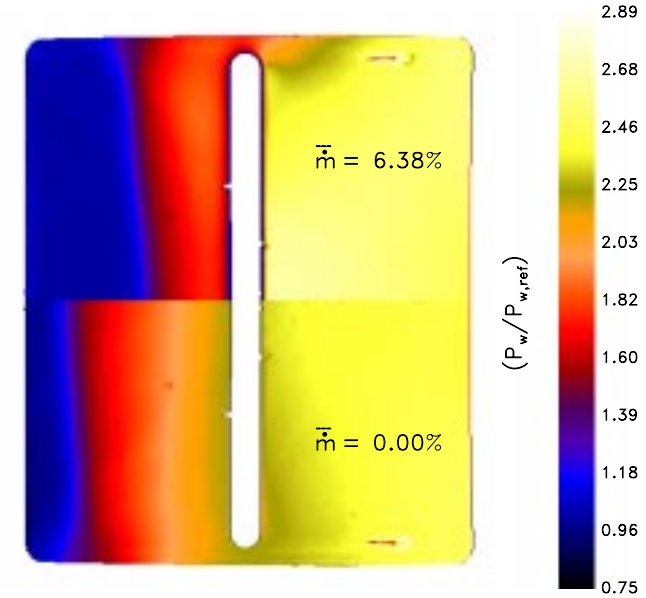

Fig. 9 Surface static pressure from pressure sensitive paint, case M246A8.

2. For both cases, there is very little difference between the distributions corresponding to the two non-zero bleed rates.
3. For the non-zero bleed cases, the pressure overshoots the inviscid pressure distribution. This overshoot in pressure is due to the barrier shock (see Fig. 1) and, as expected, is greater for the higher bleed rate case.
4. The pressure sensitive paint data agrees quite well with the conventional static tap data.
5. The drop in pressure below the inviscid value is due to the upstream influence of the expansion wave system set up by the experimental hardware (shock generator and fences).

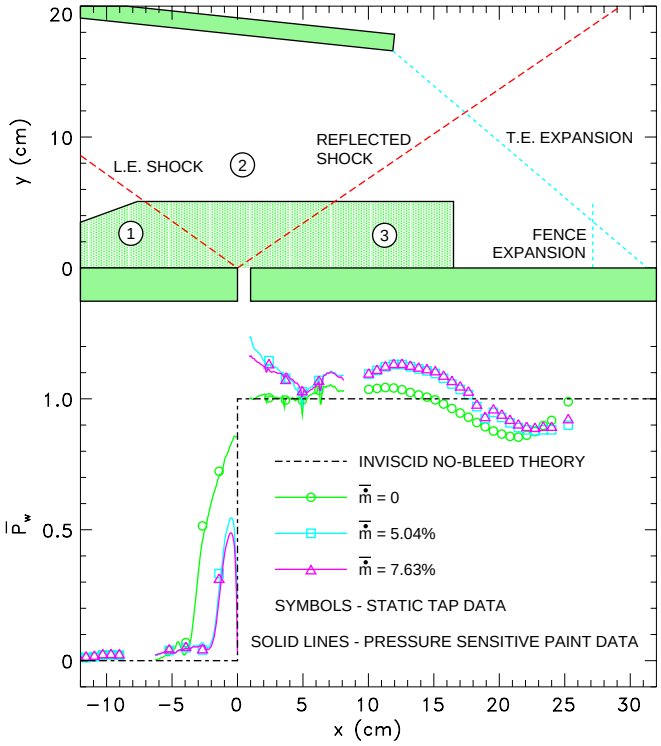

Fig. 10 Normalized centerline (z=0) static pressure distributions, case M198A6.

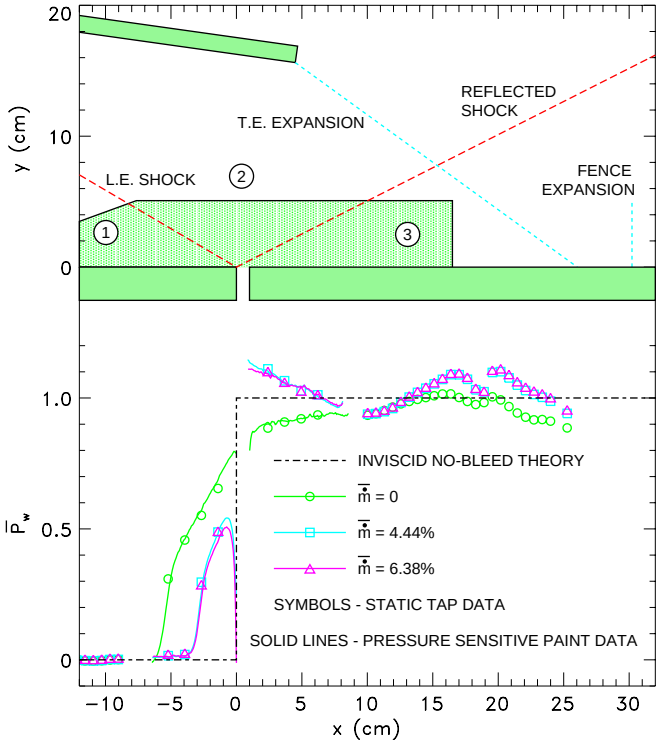

Fig. 11 Normalized centerline (z=0) static pressure distributions, case M246A8.

Flowfield Measurements in the Slot

For the flowfield measurements, only one bleed rate was considered for each of the two operating conditions. The bleed rate considered corresponds to the maximum attainable with the bleed system and is the same as the highest bleed rate condition reported for the surface static pressure data. With reference to the sonic flow coefficient distributions (Fig. 7), for all local Mach numbers, the highest flow rate attainable with the bleed sytem is always to the left of the aforementioned choke point in the flow coefficient curves.

The knife-edged static probe was used to measure the static pressure in the slot. A total of 210 points were measured at the locations shown in Fig. 12. Results from the flowfield static pressure measurements for the M198A6 and M246A8 cases are shown in Figs. 13 and 14, respectively. For presentation purposes, the data have been extrapolated to the slot surfaces by setting the pressure at the surface equal to the flowfield pressure at the first point away from the surface. The data in these plots are normalized by the wind-tunnel total pressure ($P_{t,0}$). Qualitatively, the two cases are very similar. Although undoubtedly smeared by the presence of the boundary-layer developing on the knife-edged static probe, the presence of the interior segment of the barrier shock is clearly seen by the large pressure gradient (increase) in the upper right region of the flowfield. It is not clear, however, whether the shock is attached or not. Outside this region, the static pressure is fairly uniform throughout the slot.

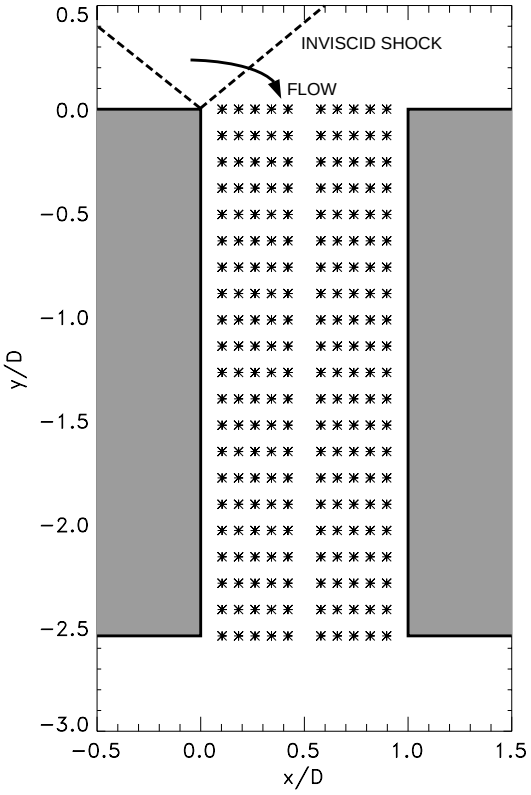

Fig. 12 Static pressure measurement grid.

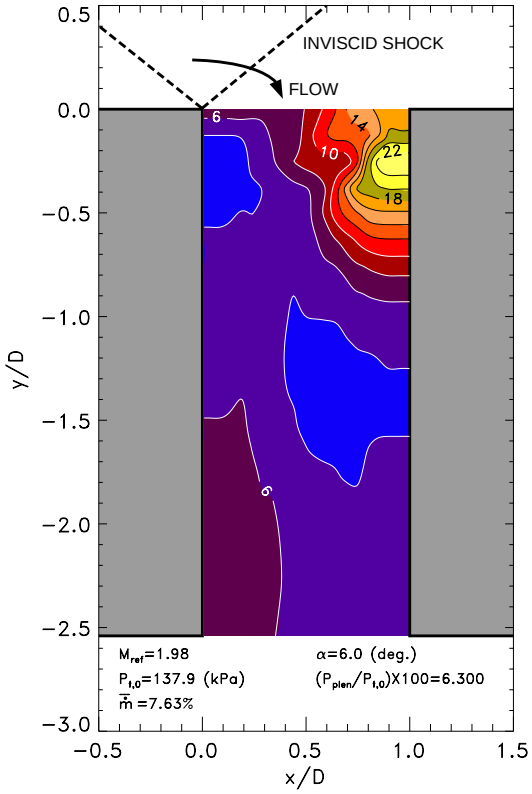

Fig. 13 Normalized static pressure distribution ($(P/P_{t,0}) \times 100$), case M198A6.

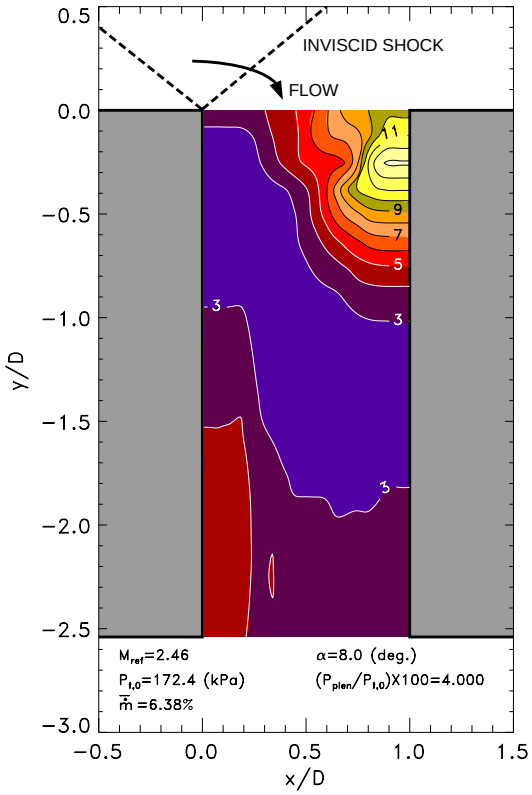

Fig. 14 Normalized static pressure distribution ($(P/P_{t,0}) \times 100$), case M246A8.

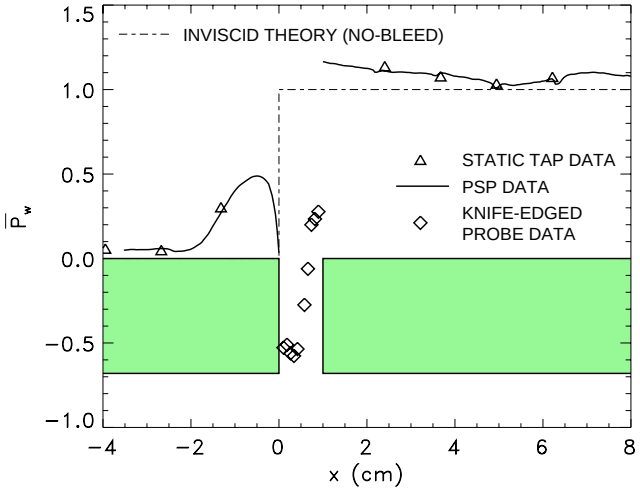

a) Case M198A6, $\overline{m}$=7.63%.

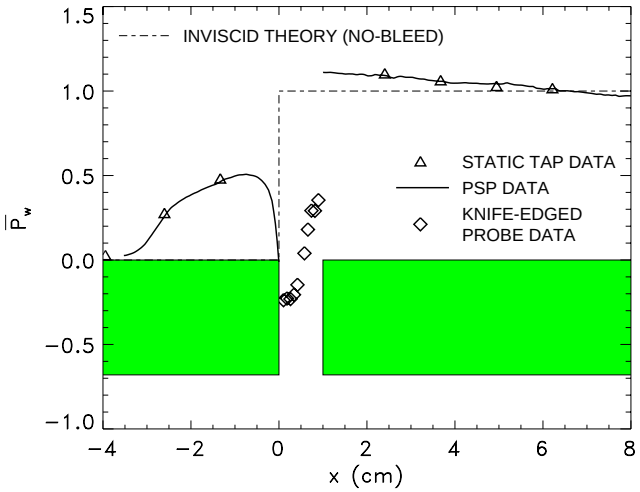

b) Case M246A8, $\overline{m}$=6.38%.

Fig. 15 Normalized centerline static pressure distributions in the y=0 plane.

The normalized static pressure distributions from the knife-edged probe in the y=0 plane are plotted along with the surface static pressure upstream and downstream of the slot in Fig. 15. The upstream influence of the slot expansion can be clearly seen in the pressure sensitive paint data. The low pressure in the upstream half of the slot opening indicates a stalled condition and that very little flow is being passed through this region.

A 0.508 mm diameter Pitot probe was used to measure the Pitot pressure in the slot. A total of 441 points were measured at the locations shown in Fig. 16. Normalized Pitot pressure distributions for the M198A6 and M246A8 cases are shown in Figs. 17 and 18, respectively. Near the top of the slot, very large flow angles relative to the Pitot probe stem are expected and the Pitot data should be considered very uncertain. This probably accounts for the lack of a discrete barrier shock in the data. Also, it should be noted that the Pitot probe will sense nearly static pressure in regions of reverse flow. These results indicate two fairly extensive regions of flow

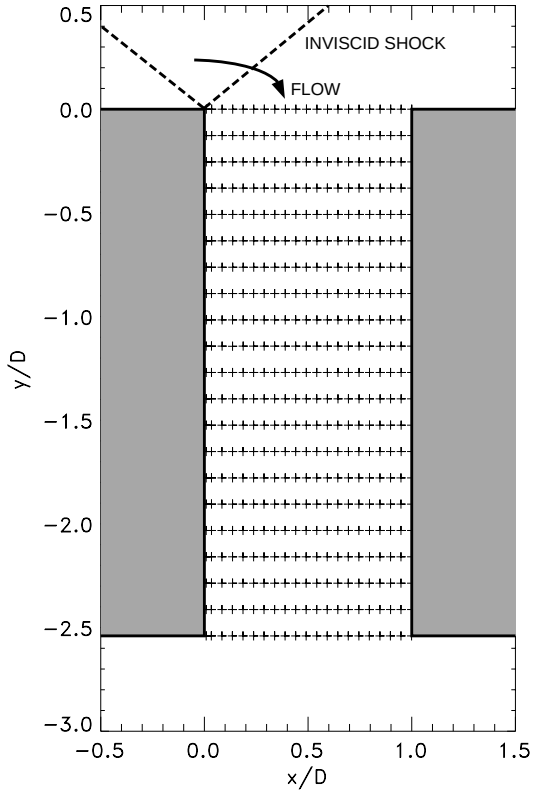

Fig. 16 Pitot pressure measurement grid.

separation in the slot which severely reduces the effective flow area. The data do indicate, however, that the flow reattaches before exiting into the bleed plenum.

The Pitot and static data were combined to calculate the local Mach number distribution in the slot. If the Pitot-to-static pressure ratio (P_{t2}/P) is less than or equal to 1.893 (subsonic flow), then the Pitot pressure is equal to the total pressure and the Mach number is calculated from the isentropic relation:

$$\frac{P_{t2}}{P} = \left(1 + \frac{\gamma - 1}{2} M^2\right)^{\frac{\gamma}{\gamma - 1}} \tag{4}$$

If the Pitot-to-static pressure ratio (P_{t2}/P) is greater than 1.893 (supersonic flow), the Mach number is calculated from the Rayleigh-Pitot tube equation:

$$\frac{P_{t2}}{P} = \frac{\left(\frac{\gamma+1}{2} M^2\right)^{\frac{\gamma}{\gamma-1}}}{\left(\frac{2\gamma}{\gamma+1} M^2 - \frac{\gamma-1}{\gamma+1}\right)^{\frac{1}{\gamma-1}}} \tag{5}$$

For purposes of the calculation, the local static pressure (P) data were interpolated onto the data grid used to acquire the Pitot data. Recall that the static pressure at the slot surface was set equal to the first column of data and recognize that this may introduce errors in the Mach number values nearest the slot surface. The calculated Mach number distributions for the M198A6 and M246A8 cases are shown in Figs. 19 and 20, respectively. The presence

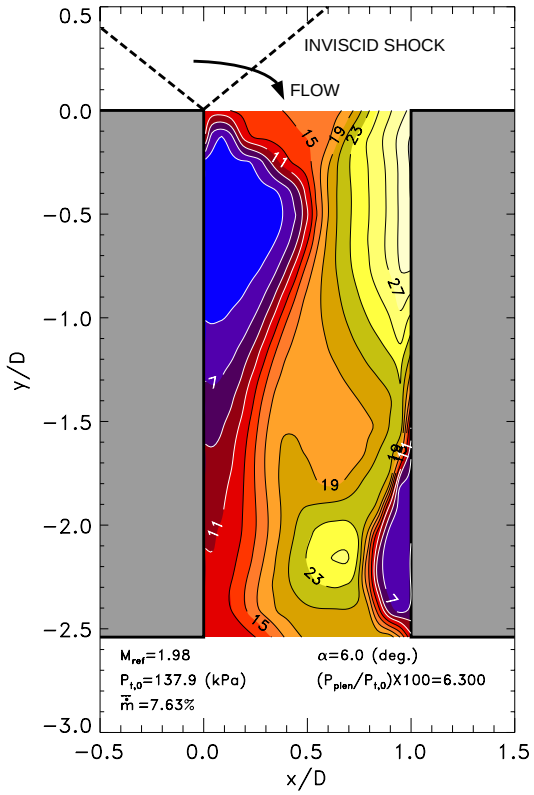

Fig. 17 Normalized Pitot pressure distribution ($(P_{t2}/P_{t,0}) \times 100$), case M198A6.

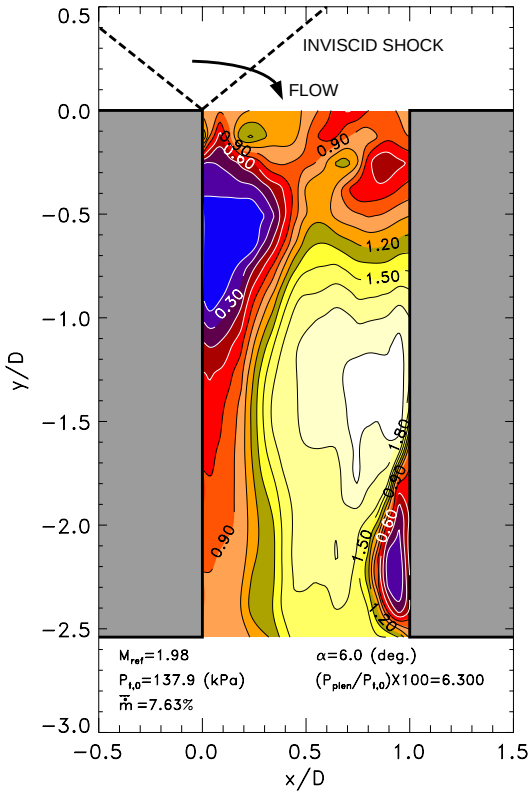

Fig. 19 Calculated Mach number distribution, case M198A6.

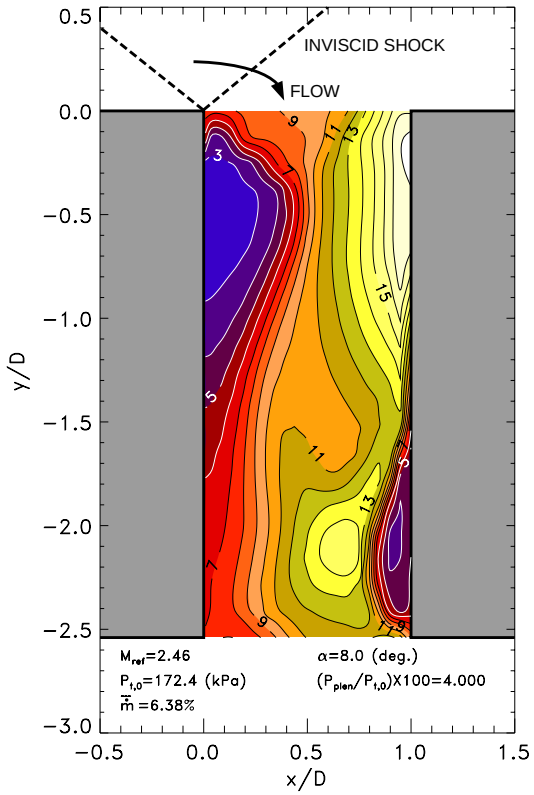

Fig. 18 Normalized Pitot pressure distribution ($(P_{t2}/P_{t,0}) \times 100$), case M246A8.

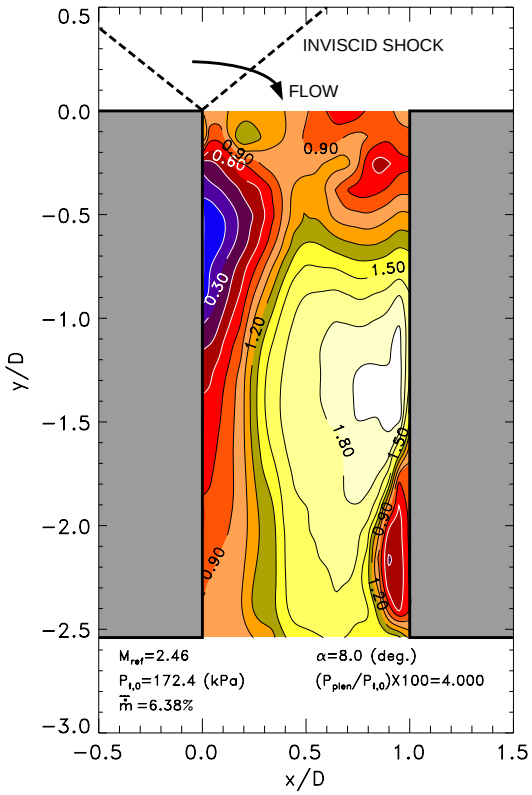

Fig. 20 Calculated Mach number distribution, case M246A8.

of the separation region on the upper left surface of the slot causes an aerodynamic convergent-divergent nozzle effect. As the flow expands downstream of the aerodynamic throat, the Mach number increases to a peak of about M=2 for both cases. The back-pressure in the plenum, however, is not low enough to maintain supersonic flow. But rather than shocking down to subsonic flow as would happen for the inviscid case, the plenum pressure feeds up through the boundary-layer on the slot surface which causes the flow to separate. Compression waves off of this separation act to decelerate the flow gradually but still the flow exits the slot supersonically. The upper separated region also leaves a rather large subsonic wake which accelerates to a near sonic condition at the slot exit.

Following Kline,[18] the propagation of the uncertainty in the measured Pitot and static pressures into the calculated Mach number was estimated from the following equation:

$$\delta M = \left[\left(\frac{\partial M}{\partial P} \delta P \right)^2 + \left(\frac{\partial M}{\partial P_{t2}} \delta P_{t2} \right)^2 \right]^{1/2} \qquad (6)$$

where δP, δP_{t2}, and δM represent the uncertainty in the static pressure, Pitot pressure, and Mach number, respectively. Using equation (6), the uncertainty in the Mach number was evaluated at each point in the flowfield and the results are shown in Fig. 21 as a function of Mach number. Note that this uncertainty includes only the pressure measurement uncertainty and not errors due to probe interference or interpolation. The results indicate that the uncertainty becomes excessive for a local Mach number less than 0.5 which is confined to relatively small regions of the flowfield.

From the surface static pressure distributions (Figs. 8 and 9), we inferred that the mass-flow distribution in the spanwise (z) direction was not uniform, but passed a higher mass-flow at the center of the slot. If we assume that the total temperature of the flow in the slot is the same as the wind-tunnel plenum, then in conjunction with the static pressure and Mach number distributions in the slot, and assuming the ideal gas law applies, we can calculate a mass-flux ($-\rho V$) distribution in the slot. Integrating the $-\rho V$ distribution along lines of constant (y) locations and then dividing by the unit mass-flow in the reference boundary-layer will yield a normalized mass-flow in the plane of symmetry:

$$\overline{\dot{m}}_{cl} = 100 \cdot \frac{\int_0^{1.0} -\rho V \, dx}{\dot{m}'_{bl,ref}} \qquad (7)$$

There are, however, at least three sources of errors to consider when performing the integration: regions of high flow angle relative to the Pitot probe stem, regions of reverse flow, and regions where the static pressure has a high gradient near the wall which makes our extrapolation assumption uncertain. The integrations were performed along the 21 rows of data and the results are shown in Fig. 22. In this plot, the centerline mass-flow calculated from equation (7) is normalized by the bulk mass-flow measured with ASME nozzle and presented as a function of y location. From this figure we can estimate that for the bulk mass-flows considered, on the average the centerline mass-flow is roughly 50% higher than the bulk mass-flow. Also the increase in centerline mass-flow through the slot indicates a significant spanwise convergence of the flow within the slot.

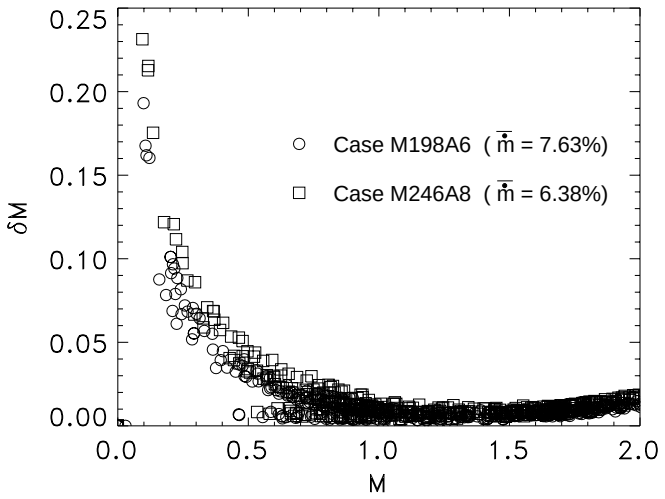

Fig. 21 Uncertainty in Mach number versus Mach number.

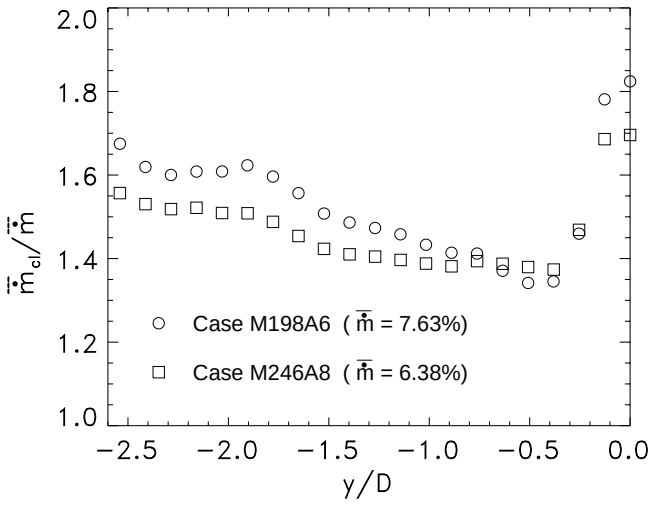

Fig. 22 Integrated mass-flow in the plane of symmetry.

Concluding Remarks

Development of global bleed models for boundary-layer control will require experimental and computational synergism due to the complexity of the flowfield. The flowfield inside a bleed slot used to control an oblique shock-wave and turbulent boundary-layer interaction has been studied experimentally. From this study we can draw the following conclusions:

1. For the configuration tested, despite a two-dimensional flowfield for the zero-bleed case, application of bleed-flow resulted in a three-dimensional flowfield. Surface static pressure data indicate that the slot passes more mass-flow near the center than at the ends. This may very well be the case in actual inlet bleed systems.
2. The flowfield in the slot is characterized by the presence of a barrier shock and two large separation regions. These features serve to reduce the flow coefficient of the bleed passage and their effects should be included in flow coefficient models.
3. Due to an aerodynamic throat effect of the separation, much of the flow through the slot is supersonic.

The data presented in this report are available from the first author on magnetic media or via the internet (fsdavis@hopi.lerc.nasa.gov).

References

[1] Delery, J. M., "Shock-Wave/Turbulent Boundary-Layer Interaction and Its Control," *Progress in Aerospace Sciences*, Vol. 22, No. 4, 1985, pp. 209–280.

[2] Hamed, A. and Shang, J. S., "Survey of Validation Data Base for Shock-Wave/Boundary-Layer Interactions in Supersonic Inlets," *Journal of Propulsion and Power*, Vol. 7, No. 4, 1991, pp. 617–625.

[3] Hamed, A. and Lehnig, T., "An Investigation of Oblique Shock/Boundary-Layer/Bleed Interaction," *Journal of Propulsion and Power*, Vol. 8, No. 2, 1992, pp. 418–424.

[4] Hamed, A., Shih, S., and Yeuan, J. J., "A Parametric Study of Bleed in Shock/Boundary-Layer Interactions," AIAA Paper 93-0294, Jan. 1993.

[5] Hamed, A., Yeuan, J. J., and Shih, S., "An Investigation of Shock Wave/Turbulent Boundary-Layer Interaction with Bleed Through Normal and Slanted Holes," AIAA Paper 93-2155, June 1993.

[6] Hamed, A., Yeuan, J. J., and Shih, S., "Flow Characteristics in Boundary-Layer Bleed Slots with Plenum," AIAA Paper 95-0033, Jan. 1995.

[7] Hamed, A., Yeuan, J. J., and Shih, S., "An Investigation of Shock Wave/Turbulent Boundary-Layer Interaction with Bleed Through Slanted Slots," AIAA Paper 93-2992, July 1993.

[8] Hahn, T. O., Shih, T. I.-P., and Chyu, W. J., "Numerical Study of Shock-Wave/Boundary-Layer Interactions with Bleed," *AIAA Journal*, Vol. 31, May 1993, pp. 869–876.

[9] Rimlinger, M. J., Shih, T. I.-P., and Chyu, W. J., "Three-Dimensional Shock-Wave/Boundary-Layer Interactions with Bleed Through a Circular Hole," AIAA Paper 92-3084, July 1992.

[10] Chyu, W. J., Rimlinger, M. J., and Shih, T. I.-P., "Effects of Bleed-Hole Geometry and Plenum Pressure on Three-Dimensional Shock-Wave/Boundary-Layer/Bleed Interactions," AIAA Paper 93-3259, July 1993.

[11] Shih, T. I.-P., Rimlinger, M. J., and Chyu, W. J., "Three-Dimensional Shock-Wave/Boundary-Layer Interactions with Bleed," *AIAA Journal*, Vol. 31, No. 10, 1993, pp. 1819–1826.

[12] Rimlinger, M. J., Shih, T. I.-P., and Chyu, W. J., "Three-Dimensional Shock-Wave/Boundary-Layer Interactions with Bleed Through Multiple Holes," AIAA Paper 94-0313, Jan. 1994.

[13] Harloff, G. J. and Smith, G. E., "On Supersonic-Inlet Boundary-Layer Bleed Flow," AIAA Paper 95-0038, Jan. 1995.

[14] Porro, A. R. and Hingst, W. R., "Use of Surface Heat Transfer Measurements as a Flow Separation Diagnostic in a Two-Dimensional Reflected Oblique Shock/Turbulent Boundary-Layer Interaction," AIAA Paper 93-0775, Jan. 1993.

[15] Bencic, T., "Experiences Using Pressure Sensitive Paint in NASA Lewis Research Center Propulsion Test Facilities," AIAA Paper 95-2831, July 1995.

[16] Bryer, D. W. and Pankhurst, R. C., *Pressure-Probe Methods for Determining Wind Speed and Flow Direction*, Her Majesty's Stationary Office, London, England, 1971.

[17] Willis, B. P., Davis, D. O., and Hingst, W. R., "Flow Coefficient Behavior for Boundary-Layer Bleed Holes and Slots," AIAA Paper 95-0031, Jan. 1995.

[18] Kline, S. J., "The Purposes of Uncertainity Analysis," *ASME Journal of Fluid Engineering*, Vol. 107, June 1985, pp. 153–160.

REPORT DOCUMENTATION PAGE

Form Approved
OMB No. 0704-0188

1. AGENCY USE ONLY (*Leave blank*)	2. REPORT DATE	3. REPORT TYPE AND DATES COVERED
	April 1998	Technical Memorandum

4. TITLE AND SUBTITLE

Flowfield Measurements in a Slot-Bled Oblique Shock-Wave and Turbulent Boundary-Layer Interaction

5. FUNDING NUMBERS

WU–505–62–52–00

6. AUTHOR(S)

D.O. Davis, B.P. Willis, and W.R. Hingst

7. PERFORMING ORGANIZATION NAME(S) AND ADDRESS(ES)

National Aeronautics and Space Administration
Lewis Research Center
Cleveland, Ohio 44135–3191

8. PERFORMING ORGANIZATION REPORT NUMBER

E–11126

9. SPONSORING/MONITORING AGENCY NAME(S) AND ADDRESS(ES)

National Aeronautics and Space Administration
Washington, DC 20546–0001

10. SPONSORING/MONITORING AGENCY REPORT NUMBER

NASA TM—1998-206974
AIAA–95–0032

11. SUPPLEMENTARY NOTES

Prepared for the 33rd Aerospace Sciences Meeting & Exhibit sponsored by the American Institute of Aeronautics and Astronautics, Reno, Nevada, January 9–12, 1995. Responsible person, D.O. Davis, organization code 5850, (216) 433–8116.

12a. DISTRIBUTION/AVAILABILITY STATEMENT

Unclassified - Unlimited
Subject Category: 02 Distribution: Nonstandard

This publication is available from the NASA Center for AeroSpace Information, (301) 621–0390.

12b. DISTRIBUTION CODE

13. ABSTRACT ***(Maximum 200 words)***

An experimental investigation was conducted to determine the flowfield inside a bleed slot used to control an oblique shock-wave and turbulent boundary-layer interaction. The slot was oriented normal to the primary flow direction and had a width of 1.0 cm (primary flow direction), a length of 2.54 cm, and spanned 16.5 cm. The approach boundary layer upstream of the interaction was nominally 3.0 cm thick. Two operating conditions were studied: M=1.98 with a shock generator deflection angle of 6° and M=2.46 with a shock generator deflection angle of 8°. Measurements include surface and flowfield static pressure, Pitot pressure, and total mass-flow through the slot. The results show that despite an initially two-dimensional interaction for the zero bleed-flow case, the slot does not remove mass uniformly in the spanwise direction. Inside the slot, the flow is characterized by two separation regions which significantly reduce the effective flow area. The upper separation region acts as an aerodynamic throat resulting in supersonic flow through much of the slot.

14. SUBJECT TERMS

Supersonic flow; Boundary layer control

15. NUMBER OF PAGES

17

16. PRICE CODE

A03

17. SECURITY CLASSIFICATION OF REPORT	18. SECURITY CLASSIFICATION OF THIS PAGE	19. SECURITY CLASSIFICATION OF ABSTRACT	20. LIMITATION OF ABSTRACT
Unclassified	Unclassified	Unclassified	